

Regular spatial structures in arrays of Bose-Einstein condensates induced by modulational instability

B B Baizakov†§, V V Konotop‡ and M Salerno†

† Dipartimento di Fisica "E.R. Caianiello" and Istituto Nazionale di Fisica della Materia (INFM), Università di Salerno, I-84081 Baronissi (SA), Italy

‡ Departamento de Física and Centro de Física da Materia Condensada, Universidade de Lisboa, Complexo Interdisciplinar, Av. Prof. Gama Pinto 2, Lisboa 1649-003, Portugal

E-mail: baizakov@sa.infn.it, konotop@cii.fc.ul.pt, salerno@sa.infn.it

Abstract. We show that the phenomenon of modulational instability in arrays of Bose-Einstein condensates confined to optical lattices gives rise to coherent spatial structures of localized excitations. These excitations represent thin disks in 1D, narrow tubes in 2D, and small hollows in 3D arrays, filled in with condensed atoms of much greater density compared to surrounding array sites. Aspects of the developed pattern depend on the initial distribution function of the condensate over the optical lattice, corresponding to particular points of the Brillouin zone. The long-time behavior of the spatial structures emerging due to modulational instability is characterized by the periodic recurrence to the initial low-density state in a finite optical lattice. We propose a simple way to retain the localized spatial structures with high atomic concentration, which may be of interest for applications. Theoretical model, based on the multiple scale expansion, describes the basic features of the phenomenon. Results of numerical simulations confirm the analytical predictions.

PACS numbers: 03.75.Fi, 03.75.-b, 05.45.Yv

Submitted to: *J. Phys. B: At. Mol. Opt. Phys.*

1. Introduction

Optical lattices formed by laser waves are the media where Bose-Einstein condensates (BEC) exhibit remarkable properties. Over the last few years there has been a significant progress in manipulation with BEC confined to optical lattices which resulted in observation of diverse new phenomena, such as coherent emission of Bose-condensed atoms [1], Bloch oscillations and Landau-Zener tunneling [2], atomic Josephson effect [3], Mott insulator - superfluid transition [4]. Realization of BEC arrays in 2D and 3D optical lattices [4,5] has opened new perspectives for investigation of fundamental properties of quantum gases in lower dimensions. Theoretical studies on the dynamics of BEC in a

§ Permanent address: Physical-Technical Institute, 2-b Mavlyanov str., 700084 Tashkent Uzbekistan

periodic potential critically rely on the concepts of band structure and Bloch states, acquired from the solid state physics. Recent developments in the field show that the above concepts, originally constructed for linear periodic systems, also play the crucial role in the physics of nonlinear periodic systems, such as BEC arrays in optical lattices [6,7,8]. A good correlation between predictions of the band theory for the BEC dynamics in a periodic potential and experimental results with static, moving, and accelerating 1D optical lattices was demonstrated in [9]. Wide range of spatiotemporal behaviour of a BEC in 1D linear- and circular-chain optical lattices in the tight-binding limit, when the dynamics is described by the discrete nonlinear Schrödinger equation, was numerically investigated in Ref. [10]. Transmission of matter wave pulses incident in a 1D optical lattice, including their collision dynamics, was theoretically considered in [11].

A subject, which is interesting both from the viewpoints of the theory and applications of BEC, is the origin and dynamics of spatially localized nonlinear excitations in the condensate confined to a periodic potential. A stimulating discovery was the proof of the existence of bright solitons in the effectively 1D BEC arrays with repulsive interaction between atoms [8,12,13]. In view of the fact that a continuous BEC with repulsive interatomic forces does not support spatially localized humps of atomic concentration, BEC arrays in optical lattices are considered to be the most inviting media for the creation and manipulation of soliton-like structures with ultracold atoms. The physical mechanism by which this possibility arises is similar to that of electrons in a periodic potential, in specific cases acquiring negative effective mass. The presence of the optical lattice can invert the sign of the dispersive term, which then balances the action of the nonlinearity. Therefore, bright solitons in BEC arrays with repulsive interaction between atoms are possible in the presence of the periodic potential of the optical lattice. It is worth to mention here that although a continuous BEC with attractive interaction between atoms can bear bright solitons, its other property leading to a collapse of the condensate at some critical atomic concentration (for review see e.g. [14]), makes it less appealing for the above purpose. In recent papers [15,16], reporting on the first experimental observation of matter-wave bright solitons in a continuous BEC with attractive interatomic forces (^7Li), the macroscopic quantum bound state of Bose-condensed atoms (bright soliton) was shown to exist in a narrow window of atomic numbers (around $\mathcal{N} \sim 5000$). Beyond that window atomic wavepackets undergo collapse or explosion. Moreover, the bright soliton with attractive forces between atoms subject to expulsive potential, as applied in [15,16], appears to be of limited lifetime due to the effect of quantum tunneling [17] (termed by authors as *quantum evaporation*), which leads to eventual explosion of the soliton. Therefore, matter-wave bright solitons composed of repulsive atoms in optical lattices, which are free of the above constraints, seem to be advantageous for applications.

Out of existing studies on localized excitations in BEC arrays, little attention has been devoted to methods of creation of such structures, so far. It has recently been suggested to employ the modulational instability, which constitutes one of the most

important phenomena associated with the evolution of nonlinear waves, to create bright BEC solitons in a 1D optical lattice [8]. A variety of localized solutions are found to the one-dimensional nonlinear Schrödinger equation with a periodic potential, some of which are spatially and temporally stable [12]. Interesting consequence of the modulational instability in a continuous BEC was reported in [18]. The authors have shown that the modulational instability leads to fragmentation of the ferromagnetic phase in a spinor Bose-condensate. Another manifestation of the modulational instability as leading to dynamical superfluid-insulator transition in a BEC confined to an optical lattice and magnetic potential has been studied in [19].

It is appropriate to mention, that the phenomenon of modulational instability is well studied in different areas of nonlinear physics, since initiated in the 1960s, by predictions in hydrodynamics [20], plasmas [21, 22], and nonlinear optics [23, 24]. For later reviews on modulational instability in Hamiltonian systems the reader is addressed to references [25, 26, 27]. In view of the existence of many features of ultracold atomic gases similar to those observed in the above mentioned systems, there is a solid ground to expect rich dynamics induced by the modulational instability in such a nonlinear system as Bose-Einstein condensates.

In the present paper we study the dynamical processes in BEC arrays confined to one-, two-, and three-dimensional optical lattices, which are due to the modulational instability. Particularly we focus on the coherent spatial structures in 2D and 3D BEC arrays, which originate from the modulational instability.

The paper is organized as follows: Section 2 contains the derivation of main equations, as well as brief exposition of the modulational instability. In section 3 we present the energy band structure for a BEC distributed over the periodic potential. In section 4 we analyze the features of spatial structures in arrays of BEC, originated from the modulational instability of the initial waveforms, corresponding to different points of the Brillouin zone. Section 5 summarizes the results of this study.

2. The multiscale analysis and modulational instability

To develop the model we consider a dimensionless 3D Gross-Pitaevskii (GP) equation

$$i\frac{\partial\psi}{\partial t} = -\Delta\psi + V(\mathbf{r})\psi + \chi|\psi|^2\psi, \quad (1)$$

where $\mathbf{r} = (r_x, r_y, r_z)$. In (1) the spatial coordinates are normalized to ℓ , ℓ being a characteristic size of the potential (say, the smallest of its periods), the time is measured in units of $2m\ell^2/\hbar$, and the amplitude of the order parameter is normalized to the total number of atoms per unit volume $\sqrt{\mathcal{N}/\ell^3}$. Then the nonlinearity coefficient χ is given by $\chi = 8\pi\mathcal{N}a_s/\ell$, where a_s is the s-wave scattering length. The potential $V(\mathbf{r})$ is assumed, for the sake of simplicity, to be separable, i.e. of the form $V(\mathbf{r}) = \sum_j V_j(r_j)$, $j = x, y, z$ (which corresponds to the majority of experimental settings), and periodic in each of the spatial directions: $V_j(r_j) = V_j(r_j + a_j)$, with a_j the period in the direction r_j (in accordance with the accepted scaling $a_j \gtrsim 1$). For convenience, the equation (1) is

considered subject to periodic boundary conditions $\psi(\mathbf{r}) = \psi(r_x + L_x, r_y, r_z)$, etc., where $L_j = N_j a_j$ with N_j and L_j respectively, the number of primitive cells and the length of the system in the direction r_j . The theory is developed for the small amplitude limit, when the multiscale analysis is applicable. Hence, we look for a solution to equation (1) in the form

$$\psi = \epsilon\psi_1 + \epsilon^2\psi_2 + \epsilon^3\psi_3 + \dots \quad (2)$$

where the ψ_j are functions of the scaled independent variables $\tau_p = \epsilon^p t$, $\xi_p = \epsilon^p \mathbf{r}$, $p = 0, 1, 2, \dots$, with ϵ a small parameter to be specified later. Denoting with $\omega_{\alpha_j}(q_j)$, and $\Phi_{\alpha_j}(r_j) \equiv |\alpha_j, q_j\rangle$, the eigenvalues and eigenfunctions of the periodic operators $\mathcal{L}_{r_j} = -\partial_{r_j}^2 + V_j(r_j)$, we have that the solution to a linear part of the equation (1), $\mathcal{L}\psi = 0$, with $\mathcal{L} = i\partial_t - \sum_j \mathcal{L}_{r_j}$, can be written in the form $|m_x m_y m_z\rangle = \prod_j \Phi_{m_j}(r_j) e^{i\omega_{\alpha_j}(q_j)t}$, with $\Phi_{m_j}(r_j)$ Bloch states of the corresponding 1D linear problems. Here m_j denotes the couple of quantum numbers $\{\alpha_j, q_j\}$, with α_j the band index and q_j the component of the wave vector in the j direction (note that the imposed boundary conditions obviously imply that $q_j \equiv q_{j,n} = \frac{2\pi}{L_j} n$ so that the extension of the Brillouin zone (BZ) in the j direction is $[-\pi/a_j, \pi/a_j]$).

Substituting the equation (2) into (1), and collecting terms of equal powers in ϵ , one arrives at the set of equations $\mathcal{L}\psi_n = \mathcal{M}_n$, with

$$\mathcal{M}_1 = 0, \quad \mathcal{M}_2 = -i\partial_{\tau_1}\psi_1 - 2\nabla_0 \nabla_1 \psi_1,$$

$$\mathcal{M}_3 = -i\partial_{\tau_2}\psi_1 - i\partial_{\tau_1}\psi_2 - \Delta_1 \psi_1 - 2\nabla_0 \cdot \nabla_1 \psi_2 - 2\nabla_0 \cdot \nabla_2 \psi_1 + \chi |\psi_1|^2 \psi_1,$$

where ∇_p denotes the gradient with respect to ξ_p .

Since we are interested in instabilities of the condensate wavefunction, we investigate the influence of the nonlinear term in the equation (1) on the Bloch states of the underlying linear problem. To this end we take as starting point in the expansion (2), a modulated state of the form

$$\psi_1 = \mathcal{A}(\xi_1, \dots; \tau_1, \dots) e^{-i\omega_0 \tau_0} |m_{0x} m_{0y} m_{0z}\rangle, \quad (3)$$

with $\omega_0 \equiv \sum_j \omega_{\alpha_0, j}(q_j)$ (the subscript zero refers to the chosen band, below we consider the two lowest ones). Then the first order equation is automatically satisfied by ψ_1 , while the equation of the second order can be solved in the form

$$\psi_2 = \sum_{\alpha}' \mathcal{B}_{\alpha} e^{-i\omega_0 \tau_0} |\alpha_x, q_{0,x}; \alpha_y, q_{0,y}; \alpha_z, q_{0,z}\rangle, \quad (4)$$

where the prime denotes $\alpha \neq \alpha_0$ in the sum and have taken into account that the terms with $\mathbf{q} \neq \mathbf{q}_0$ give zero contribution. Analysis similar to that of reference [8] shows that $\mathcal{A} = \mathcal{A}(\mathbf{R}; \xi_2, \dots; \tau_2, \dots)$ with $\mathbf{R} = \xi_1 - \mathbf{v}\tau_1$ and $\mathbf{v} = -\langle \alpha_{0x} \alpha_{0y} \alpha_{0z} | 2i\nabla | \alpha_{0x} \alpha_{0y} \alpha_{0z} \rangle$ is the group velocity of the carrier wave. The coefficients \mathcal{B}_{α} are found as

$$\mathcal{B}_{\alpha} = \frac{\Gamma_{\alpha_x, \alpha_0, x}^{(y,z)} \partial_{x_1} \mathcal{A} + \Gamma_{\alpha_y, \alpha_0, y}^{(x,z)} \partial_{y_1} \mathcal{A} + \Gamma_{\alpha_z, \alpha_0, z}^{(x,y)} \partial_{z_1} \mathcal{A}}{\omega_0 - \omega_{\alpha}(\mathbf{q}_0)}, \quad (5)$$

where $\omega_\alpha(\mathbf{q}_0) = \sum_j \omega_{\alpha_j}(q_{0j})$, $\Gamma_{\alpha_x, \alpha_{0,x}}^{(y,z)} = -\langle \alpha_x, q_{0,x} | 2\partial_{x_0} | \alpha_{0,x}, q_{0,x} \rangle \delta_{\alpha_y, \alpha_{0,y}} \delta_{\alpha_z, \alpha_{0,z}}$ (other coefficients Γ are obtained by cyclic permutations of x, y, z). Finally, considering the orthogonality of \mathcal{M}_3 to $|m_{0x}m_{0y}m_{0z}\rangle$ we obtain the following 3D NLS for the slowly varying envelope

$$i \frac{\partial \mathcal{A}}{\partial \tau_2} + \frac{1}{2} \sum_{j=x,y,z} \mathbf{M}_{\alpha_j, jj}^{-1} \frac{\partial^2 \mathcal{A}}{\partial R_j^2} - \tilde{\chi} |\mathcal{A}|^2 \mathcal{A} = 0, \quad (6)$$

where we assumed \mathcal{A} not depending on ξ_2 , and introduced the inverse of the effective mass tensor

$$\frac{1}{2} \mathbf{M}_{\alpha_j, jj}^{-1} = 1 + \sum_{\alpha_x} \frac{|\Gamma_{\alpha_x \alpha_{0,x}}^{(y,z)}|^2}{\omega_{\alpha_x}(q_{0,x}) - \omega_{\alpha_{0,x}}(q_{0,x})} = \frac{1}{2} \partial_{q_j}^2 \omega_{\alpha_j}(\mathbf{q}), \quad (7)$$

and the effective nonlinearity

$$\tilde{\chi} = \chi \prod_{j=x,y,z} \int_0^{L_j} |\Phi_{m_{0j}}|^4 dr_j. \quad (8)$$

Now we are at the point to discuss the small parameter. To simplify, we consider a cubic box with $a_j = \ell$ and $L_j = L$. On the one hand, as it was mentined above, the physical order parameter is normalized to the total number of atoms \mathcal{N} , while the formal wave function ψ must be normalized to one: $\int |\psi|^2 d\mathbf{r} = 1$. On the other hand all parameters in the equation (6) must be of order one. Next we notice the oscillatory character of the Bloch functions, in a general situation leads to the fact that the integrals in the last expression (8) for $\tilde{\chi}$ has a numerical smallness (see e.g. the examples below). Then, taking into account that $\chi = 8\pi \mathcal{N} a_s / \ell$ one can define $\epsilon = \mathcal{N} a_s \ell^2 / L^3$. Consider now a condensate with $\mathcal{N} = 10^5$ of ^{87}Rb atoms ($a_s \approx 5.5$ nm) homogeneously distributed over a cubic box with $L = 100 \mu\text{m}$ having $N_i = 100$ cells in each direction (respectively $\ell = 1 \mu\text{m}$). Then we compute $\epsilon \approx 0.014$. A physical situation when ϵ is not too small (say in experiments [5] it can be identified as $\epsilon \approx 0.257$) the multiple scale expansion, strictly speaking, is not valid. For this reason below we employ the numerical simulations, which, however, clearly illustrate that the small amplitude limit gives remarkably good estimates for the characteristic scales of the problem and allows one to understand the symmetry of the developed patterns.

Let us analyze the stability problem within the framework of equation (6), i.e. look for a solution of the form (3) with $\mathcal{A} = (\rho + a e^{i(\Omega \tau_2 - \mathbf{K} \mathbf{R})} + b e^{-i(\Omega \tau_2 - \mathbf{K} \mathbf{R})}) e^{-i \rho^2 \tau_2}$, where $|a|, |b| \ll \rho$. This solution is modulationally unstable if

$$Z(Z + 4\tilde{\chi}\rho^2) < 0, \quad Z = \sum_{j=x,y,z} \mathbf{M}_{\alpha_j, jj}^{-1} K_j^2, \quad (9)$$

where the modulational instability is understood in the sence of a plain wave instability with respect to small modulations of its amplitude. Below in section 4 we consider the modulational instability of solutions to equation (1) in the form of Bloch states induced by periodic small amplitude and long-wavelength perturbation.

3. Energy band structures

In the previous section we assumed the knowledge of the Bloch states and energy bands of the underlying linear Schrödinger problem. For generic multidimensional potentials this could be a quite difficult problem to solve. To avoid difficulties we shall restrict here to the case of separable potentials of trigonometric form i.e. we take $V(\mathbf{r}) = \sum_j V_j(r_j)$, $j = x, y, z$ with $V_j(r_j)$ given by

$$V_j(r_j) = A \cos(\kappa_j r_j). \quad (10)$$

Here A is a constant fixing the depth of the lattice and $2\pi/\kappa_j$ the periodicity in the r_j directions. In the following we fix $\kappa_j = 2$ for all j so that the potential will be a superposition of identical one dimensional Mathieu potentials, and the corresponding Bravais lattice will have simple cubic symmetry. The band structure and the Bloch states of the linear Schrödinger equation are then obtained as

$$E_\alpha(\mathbf{k}) = \sum_j \epsilon_\alpha(\mathbf{k}_j), \quad \Psi_\alpha(\mathbf{k}, \mathbf{r}) = \prod_j \varphi_\alpha(\mathbf{k}_j, \mathbf{r}_j), \quad (11)$$

where α denotes the band index and $\epsilon_\alpha(k_j)$ and $\psi_\alpha(k_j, r_j)$ are the eigenvalues and eigenfunctions of the Mathieu equation

$$-\frac{d^2 \varphi_{k,\alpha}}{dx^2} + A \cos(2x) \varphi_{k,\alpha} = E_\alpha(k) \varphi_{k,\alpha}. \quad (12)$$

This equation can be transformed, making use of the expansion of the wave function into momentum eigenfunctions (Fourier expansion), into a tridiagonal problem whose solutions can be obtained with high accuracy by means of continued fractions. As an example of these calculations we report in figure 1 the first two energy bands of the 2D separable Mathieu potential, in the case $A = 1$ (note that with the choice $\kappa = 2$ the potential has periodicity π in both directions, so that the BZ is a square of size 2).

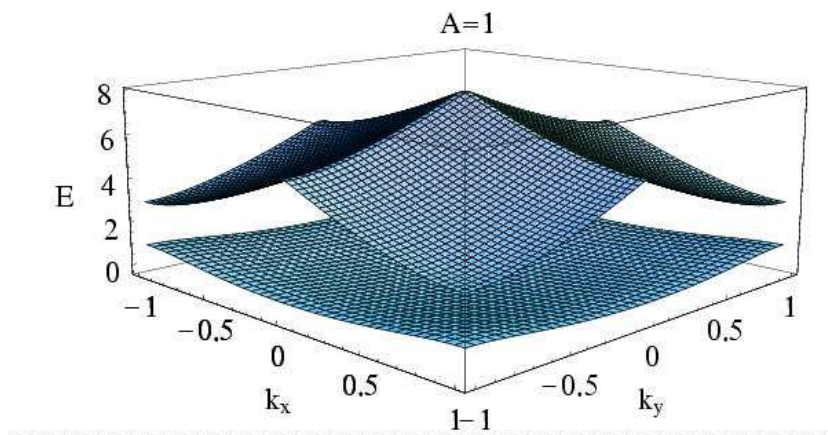


Figure 1. The first two bands of the 2D separable Mathieu potential of amplitude $A = 1$ and lattice constants $a = b = \pi$ plotted in the reduced zone scheme.

In figure 2 we also show the sections of constant energy for the bands depicted in figure 1. By changing the amplitude of the potential the band structure will change,

and the bands become more flat and more separated as the amplitude of the potential is increased. In figures 3,4 we show the contour plots of Bloch states at different points

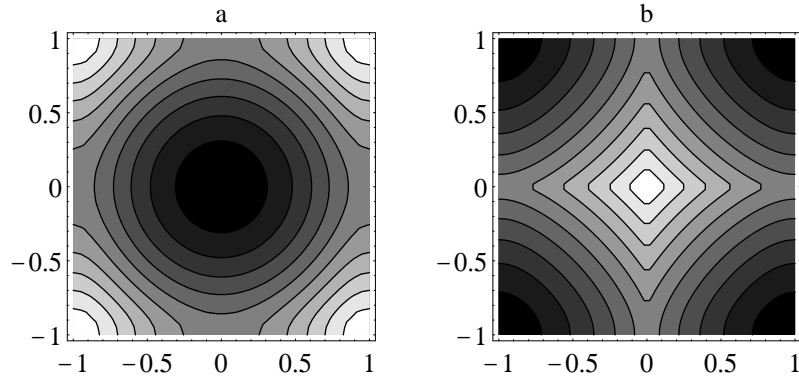


Figure 2. Sections of constant energy for the lower (a) and upper (b) bands in figure 1. The white regions denote areas of higher energy.

in the BZ. We remark that, due to the separability of the potential, both the derivative

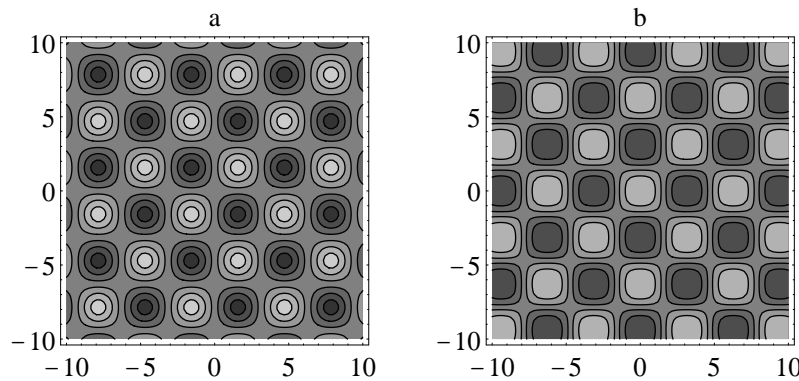


Figure 3. Contour plots of the Bloch states at the corner $k_x = 1, k_y = 1$ of the BZ for the lower (a) and upper (b) band of figure 1. The wavefunction in (a) leads to soliton formation through modulational instability while the one in (b) is modulationally stable.

and the curvature of the band are independent on k_y (respectively k_x) for fixed values of k_x (respectively k_y) in the BZ. This is seen in figure 5, where the group velocity and the components of the reciprocal mass tensor are reported for the bands in figure 1. Similar calculations can be easily done for the 3D separable Mathieu potentials. The analysis can be extended to lattices with rectangular or tetragonal symmetry, as well as, to more general separable potentials such as the ones considered in [28].

In the following sections we shall use these results to compare numerical studies of the instability of Bloch states in presence of nonlinear interactions with the prediction (equation (9)) of the previous section.

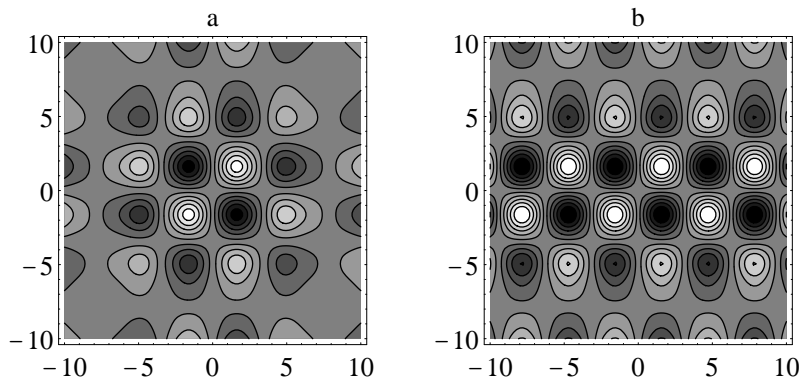


Figure 4. Contour plots of Bloch states of the lower band along lines of symmetry of the BZ. Case (a) refers to $k_x = 0.8, k_y = 0.8$ while (b) to $k_x = 1.0, k_y = 0.8$.

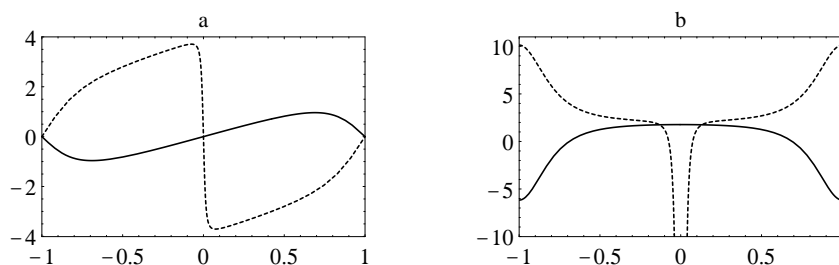


Figure 5. The group velocity (a) and the reciprocal of the effective mass ω_{xx} (respectively ω_{yy}) (b), as a function of k_x (respectively k_y), for arbitrary k_y (respectively k_x) in the BZ. The continuous and broken lines refer, correspondingly, to the first and second band of figure 1 (notice from (a) that there is no singularity for ω_{xx} (or ω_{yy}) in the origin).

4. Numerical simulations

The linear stability analysis, described in section 2 gives the growth rates and spectra for the modulational instability. This information appears to be sufficient to predict the spatial arrangement and symmetry of the emerging soliton-like structures. However, to gain more insight into the development of modulational instability one has to recourse to numerical simulations.

For the numerical study we have used the potential $V_j(r_j) = A \cos(\kappa r_j)$ for $j = x, y, z$, which is motivated by the recent experiments [4, 5]. Then in the above formulas the terms corresponding to $j = x$, $j = x, y$, and $j = x, y, z$ are retained, respectively for 1D, 2D and 3D optical lattices. Also in the case at hand $\mathbf{M}_{\alpha,xx}^{-1}$, $\mathbf{M}_{\alpha,yy}^{-1}$, and $\mathbf{M}_{\alpha,zz}^{-1}$ have the same functional dependence on the arguments, which means that they coincide when $q_x = q_y = q_z$. Numerical solution of the equation (1) has been performed by the operator splitting procedure using multi-dimensional fast Fourier transform [32]. The spatial domain $x, y, z \in [-\frac{L}{2}, \frac{L}{2}]$ (i.e. $L_x = L_y = L_z = L$) was represented by an array of 128 x 128 x 128 points. For 1D and 2D cases the results were checked by increasing the number of grids (512 and 256 x 256 respectively), which

showed no qualitative difference. The time step was $\delta t = 0.001$. To be specific, we concentrate on the case of positive scattering length, $\chi = 1.0$, choose $\kappa = 2.0$ (i.e. $a_x = a_y = a_z = \pi$), and $\rho = 0.5$.

4.1. 1D optical lattice

Basic features of the development of modulational instability and formation of soliton-like excitations in effectively 1D optical lattice was described in [8,12]. Below we extend the parameter values, which can lead to formation of qualitatively different types of localized excitations.

The coefficient of nonlinearity χ in equation (1) is an important parameter which determines such a property of BEC as the macroscopic quantum self-trapping [29,30,31]. At strong nonlinearity the tunneling of atoms between adjacent wells of the optical lattice is suppressed, despite the significant population imbalance, due to macroscopic quantum self-trapping effect. This property affects the development and further evolution of spatially localized excitations in BEC arrays. In figure 6 we report two types of soliton-like excitations, developed in 1D BEC arrays at weak and strong nonlinearities. All remaining parameters, except χ , are similar in these two cases. Envelope soliton-like modes, which occupy few lattice sites are formed at weak nonlinearity, while the intrinsic localized modes, occupying a single lattice site are formed at strong nonlinearity. The time required for development of these excitations are also different. The localized

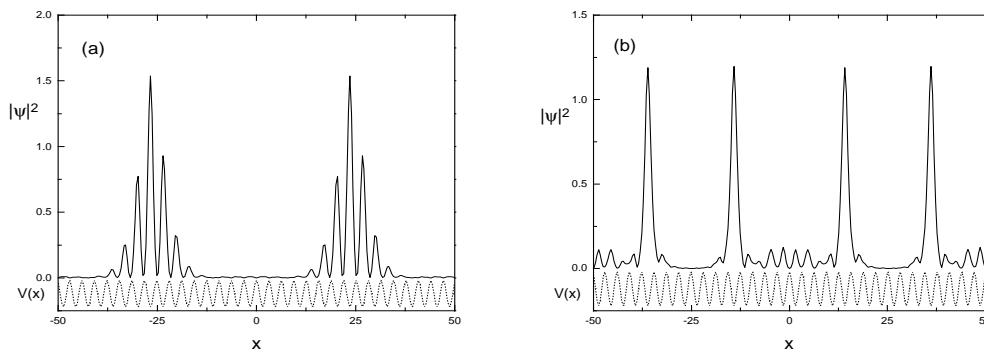


Figure 6. Two types of soliton-like excitations in arrays of BECs confined to 1D optical lattice, emerging due to the modulational instability of the initial waveform $\psi(x,0) = 0.5 \sin(x)$ at $t = 0$. The lower curve represents the optical lattice potential $V(x) = A \cos(\kappa x)$. (a) Envelope solitons, occupying few lattice sites, are formed at $t = 400$ when the nonlinear atomic interactions are weak $\chi = 0.2$. (b) Intrinsic localized modes, which fit a single lattice site, are formed at $t = 70$ for strong nonlinearity $\chi = 1.0$. Parameter values $A = 1.0$, $\kappa = 2.0$, $L = 32\pi$. The initial waveform is perturbed by $\delta\psi(x) = 0.01 \sin(0.125x)$

excitations represented in the figure 6 are thin disks filled in with BEC atoms, where the atomic density is much greater than in neighbouring array sites. The dynamics of these excitations is governed by the 1D nonlinear Schrödinger equation [8], and for particular parameter settings they can be stable [12], or have very long (relative to duration of

experiments) recurrence times. The separability of the periodic lattice potential in equation (1) leads to similar scenarios of the development of modulational instability also in 2D and 3D cases considered below.

4.2. 2D optical lattice

Now let us consider in more detail the development of soliton-like excitations and the possibility to stabilize them in a 2D optical lattice. A 2D optical lattice is formed by overlapping two laser standing waves along the x and y axes, superimposed on a continuous BEC in a magnetic trap. The condensate is then fragmented and confined in many narrow tubes centered at lattice potential minima and directed along the z axis. As a result of modulational instability, the initial distribution of the atomic density over the tubes in the optical lattice is changed.

In order to analyze the instability of initial waveforms we consider Bloch states corresponding to different points of the BZ. Let us consider the points $\mathbf{q}_0 = (\pm 1, \pm 1)$ at the boundary of the BZ (figure 1). Then, restricting consideration to the two lowest bands ($\alpha = 1, 2$), one can distinguish three different cases:

4.2.1. Case 1. Both eigenfunctions $|m_{0,x}\rangle$ and $|m_{0,y}\rangle$ belong to the first lowest zone: $m_{0,x} = m_{0,y} = (1, \pm 1)$. Then $\mathbf{M}_{1,xx}^{-1} = \mathbf{M}_{1,yy}^{-1} = \mathbf{M}_1^{-1} < 0$ and the wave is unstable. The BEC population dynamics in this case is reported in figure 7. The most interesting feature of the modulational instability developed is that it evolves in a *regular* structure which represents symmetrically spaced localized in space (we call them soliton-like) distributions (see figure 7b). Each of the humps shown in the figure represents a tightly confined tube along the z -direction. The number of tubes is proportional to the size of the box. In order to illustrate the last statement we performed calculations (see figure 8) with parameter settings similar to those of figure 7 with the exception of domain size $L = 28\pi$.

In order to understand this behavior we notice that from the equation (9) we get that the excitations with characteristic scales $\lambda > \lambda_{min} = \frac{2\pi}{K_{max}} = \frac{\pi}{\rho} \sqrt{\frac{|\mathbf{M}_1^{-1}|}{\tilde{\chi}}}$, where \mathbf{M}_1^{-1} is the inverse of the effective mass tensor, are unstable. The largest increment (i.e. the large $\text{Im}|\Omega|$) is achieved for $\lambda_0 = \sqrt{2}\lambda_{min}$. This has two consequences. First, the symmetry group of the developed structure must be of C_n type with the symmetry axis coinciding with that of the condensate, and second, an effective scale $\lambda_{eff} \sim \lambda_0$ must be a characteristic scale of the most excitation which at the beginning of the evolution. One can estimate the value of λ_0 taking into account that for a chosen point of BZ the inverse of the effective mass tensor is $|\mathbf{M}_1^{-1}| \approx 6$ (see figure 5) and for the solutions studied numerically the effective nonlinearity is $\tilde{\chi} \approx 0.1935$ (the respective normalized eigenfunctions are approximated by $\frac{2}{\pi} \sin(x)$ [8], which gives $\lambda_0 \approx 20.053$. This result corroborates with the distances between the humps along the radial direction measured from the direct numerical simulations: $\lambda_{eff} \approx 23.0$ (figure 9). Next we have to take into account that the carrier wave mode is chosen at the point $\mathbf{q} = (\pm 1, \pm 1)$ placed at the

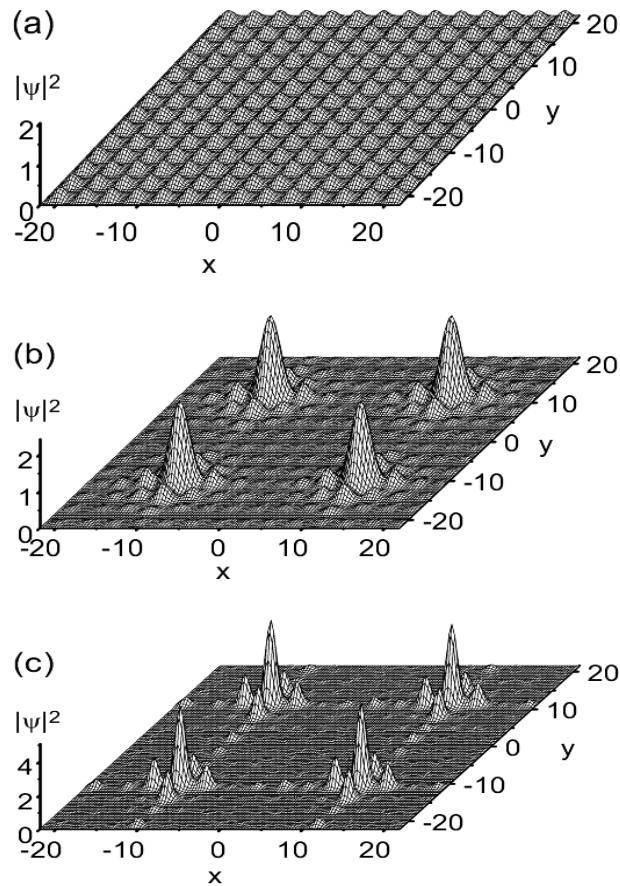


Figure 7. The evolution of BEC atomic distribution in a 2D optical lattice according to equation (1) with $A = 1.0$, $\kappa = 2.0$, $\chi = 1.0$, $L = 14\pi$. (a) The initial waveform $\psi(x, y, 0) = 0.5 \sin(x) \sin(y)$ at $t = 0$. (b) Formation of soliton-like excitations due to modulational instability at $t=85$ when the initial waveform is perturbed by $\delta\psi(x, y) = 0.01 \sin(0.125x) \sin(0.125y)$. (c) The distribution (b) slightly narrows but remains stable for very long times when the strength of the trap potential is adiabatically increased up to $A = 3.0$ during $85 < t < 90$. The snapshot (c) is shown at $t = 200$ (stability is verified up to $t=1000$).

corner of the BZ which corresponds to waves whose phases propagate in the directions $x = \pm y$. This immediately specifies the symmetry C_4 . In other words, one can specify the points where the humps (confined tubes) should appear: in the plane (x, y) these are intersections of lines $x = \pm y$ with the circles of radii $(\frac{1}{2} + p) \lambda_{eff}$ where $p = 0, 1, \dots$. In a square box of size L one will observe L^2/λ_{eff}^2 humps. This estimate being rather rough (it does not take into account boundary effects) was confirmed by our numerical simulations. Also one can predict that the characteristic diameters of the humps should be less than λ_{min} (≈ 7.1 in our case). This gives an estimate for the BEC density in a tube n_t versus the initial density n_0 : $n_t = \frac{L_x L_y}{\lambda_{min}^2} n_0$, which in our case gives $n_t \approx 38n_0$. In order to evaluate the increase of the BEC atomic density in a soliton-like excitation, we have numerically integrated $|\psi(x, y, t)|^2$ at $t = 85$ (figure 7b) over individual lattice sites. The result is that 65 % of the BEC matter, initially uniformly distributed over the

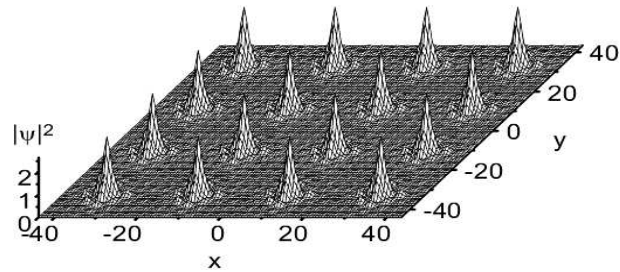


Figure 8. Regular spatial structures with BEC in a 2D optical lattice, emerged due to modulational instability. Parameter settings are similar to those of figure 7, except the domain size $L = 28\pi$.

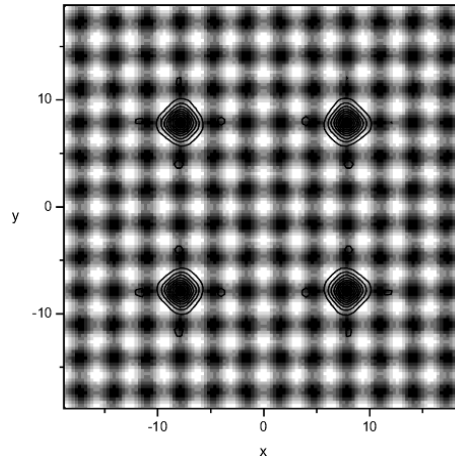


Figure 9. Contour plot of localized excitations superimposed on the profile of the optical lattice potential, showing that each excitation fits a single cell. Dark regions correspond to the minima of the periodic potential for $L_x = L_y = 12\pi$.

optical lattice, are collected in four sites due to the modulational instability. Therefore, the increase of the atomic density in a localized excitation is $n_t = \frac{196}{4} \cdot 0.65 \cdot n_0 \simeq 32n_0$, which is close to the above analytical estimation. For the 3D case considered in the next subsection this last estimate for the BEC density in hollows n_h is modified as:
$$n_h = \frac{L_x L_y L_z}{\lambda_{min}^3} n_0.$$

As we have seen, the modulational instability results in formation of regular pattern of soliton-like excitations in arrays of BEC (figures 7b, 8). However, they eventually decay in accordance with equation (6), which does not support stable solitonic solutions in 2D and 3D. A simple way to retain these excitations would be the increasing of the strength of the periodic trap potential, when excitations are formed. High potential barrier between lattice sites then suppresses the atomic tunneling, providing strong confinement. This idea is illustrated in figure 10, where we show the evolution of the BEC atomic distribution. Until $t = 85$ the dynamics is guided by the modulational instability, resulting in formation of regular spatial structures with BEC. As the soliton-

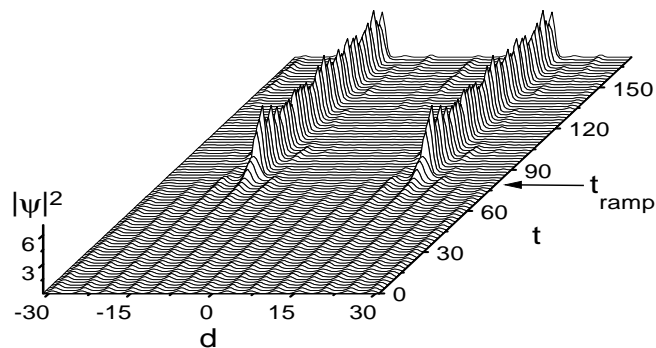


Figure 10. Evolution of the BEC distribution corresponding to figure 7, shown as a diagonal section. d is a distance along the diagonal of the square domain with $L = 14\pi$.

like excitations are formed, the strength of the optical lattice was increased adiabatically, starting at $t = 85$ and ending at $t = 90$, according to law $A(t) = 2[1 - \frac{1}{2} \cos(\frac{\pi(t-t_{\text{ramp}})}{\Delta t})]$, where $t_{\text{ramp}} = 85$, $\Delta t = 5$. To obtain estimates in physical units recall that time is normalized to $\frac{2m}{\hbar k_L^2} = 50\mu\text{s}$ (for ^{87}Rb atoms and $k_L = 8.06 \cdot 10^{-6} \text{ m}^{-1}$), and the strength of the periodic potential is expressed in units of recoil energy $E_r = \frac{\hbar^2 k_L^2}{2m}$. Therefore, $t = 85$ corresponds to $\sim 4 \text{ ms}$, while $A = 1.0$ corresponds to $\sim E_r$. These values are typical in experimental situations.

To understand the stabilization phenomenon we notice that λ_{min} is of order of $2a_x$ ($2a_y$), which means that the most of BEC atoms are concentrated in a unique cell (see figure 9). This type of excitations closely resemble the intrinsic localized modes in BEC in the tight-binding approximation [33,34]. By increasing the potential amplitude one makes the optical lattice more deep, which in turn leads to decreasing both the probability of tunneling of atoms from the most populated cell to neighbor cells and a "number" of atoms in classically forbidden zone. As a consequence, the BEC density in the most populated cell is growing, which is illustrated by figures 7c and 10.

4.2.2. Case 2. The eigenfunctions $\Phi_{m_0,x}$ and $\Phi_{m_0,y}$ belong to different zones, say $\Phi_{m_0,x}$ belongs to the first lowest zone: $m_{0,x} = (1, \pm 1)$ and $\Phi_{m_0,y}$ belongs to the second lowest zone: $m_{0,y} = (2, \pm 1)$. Then $\mathbf{M}_{1,xx}^{-1} < 0$ and $\mathbf{M}_{1,yy}^{-1} > 0$, and the condensate is unstable.

In this case the instability condition takes the form $0 < \mathbf{M}_{2,yy}^{-1} K_y^2 - |\mathbf{M}_{1,xx}^{-1}| K_x^2 < 4\tilde{\chi}\rho^2$, and the most unstable excitations have $K_x^2 < \frac{\mathbf{M}_{2,yy}^{-1}}{|\mathbf{M}_{2,xx}^{-1}|} K_y^2$ (which is related to the fact that an eigenfunction $\Phi_{m_0,x}$ belongs to the "unstable" branch). That is why the main instability results in a pattern having different symmetry: it develops in the x -direction. Along this direction the pattern is rapidly split in a sequence of solitary waves. The instability develops also along y -direction, but at much larger time scales (see figure 11). To estimate the number of humps, we take into account that the periodic boundary conditions impose a characteristic scale $K_x = 2\pi/L$ which leads to the following estimate for the most unstable scale λ_0 , and thus to λ_{eff} : $\lambda_0 \approx 2\pi/\sqrt{\frac{2\pi}{L} - \frac{2\tilde{\chi}\rho^2}{\mathbf{M}_1^{-1}}}$. For the case, illustrated in figure 11a we obtain $\lambda_0 \approx 24$, which yields for the number of humps in the

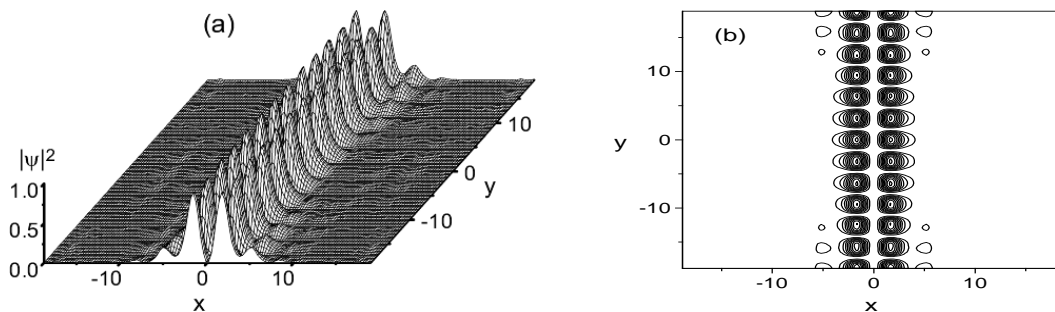


Figure 11. Distribution of BEC in a 2D optical lattice with $A = 1.0$, $\kappa = 2.0$, $\chi = 1.0$, $L = 12\pi$ subject to the initial condition $\psi(x, y, 0) = 0.5 \sin(x) \cos(y)$. (a) Regular pattern of soliton-like excitations are formed at $t = 32$. (b) Contour plot of localized excitations showing that they occupy the sequence of single lattice sites along the y direction.

x direction $LK_{max}/2\pi \sim L/\lambda_0 \sim 2$. The instability is developed in y -direction as well, which is characterized by much larger spatial and temporal scale, and for experimental purposes can be neglected. In order to preserve the developed spatial structures with high atomic density, it would be enough to increase the strength of the periodic trap potential, since the excitations fit the sequence of single lattice cells along the y direction (figure 11b).

4.2.3. Case 3. Both eigenfunctions $\Phi_{m_{0,x}}$ and $\Phi_{m_{0,y}}$ belong to the second lowest zone: $m_{0,x} = m_{0,y} = (2, \pm 1)$. Then $\mathbf{M}_{2,xx}^{-1} = \mathbf{M}_{2,yy}^{-1} > 0$ and the wave is stable, which was confirmed numerically using the initial conditions $\psi(x, y, 0) = 0.5 \cos(x) \cos(y)$.

4.2.4. Other points of the Brillouin zone. It is of particular interest for applications to explore the development of modulational instability of initial waveforms, corresponding to different points of BZ. We have tried the Bloch states with wavevectors spanning the first BZ. The main observation from the relevant numerical simulations is that, the modulational instability results in formation of different spatial structures with BEC depending on the initial waveform. The time required to formation of these structures is also different.

As an example, in figure 12 we report the result of modulational instability of the Bloch state with $m_{0,x} = m_{0,y} = (0.9, \pm 0.9)$. This initial distribution seems to be of interest because it resembles the situation, when a BEC of comparatively small size is loaded into the optical lattice, so that minor number of lattice sites are filled in with BEC, others being almost empty. In this case the cells in the central part of the optical lattice contain more BEC atoms, than the peripheral ones. The localized excitations developed due to the modulational instability occupy the central nearest-neighbor lattice cells.

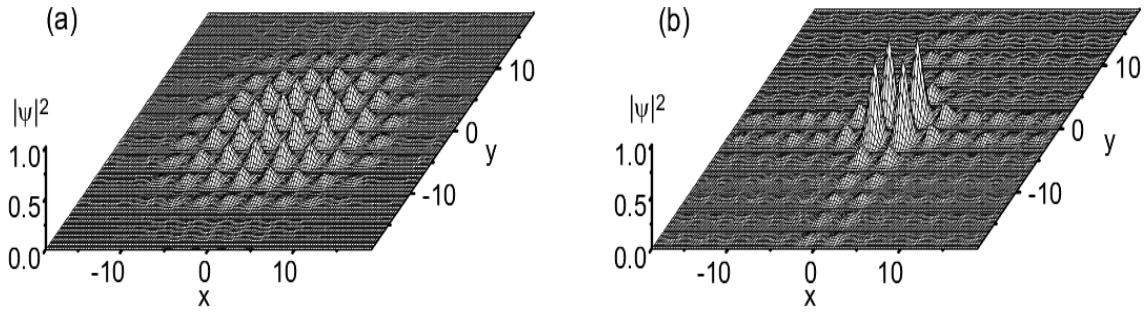


Figure 12. Redistribution of the BEC atomic population in a 2D optical lattice due to modulational instability. $A = 1.0$, $\kappa = 2.0$, $\chi = 1.0$, $L = 12\pi$ (a) The initial waveform, corresponding to the Bloch state $m_{0,x} = m_{0,y} = (0.9, \pm 0.9)$. (b) Formation of soliton-like excitations due to modulational instability at $t = 16$.

4.3. 3D optical lattice

Qualitatively similar behaviour of the modulational instability with respect to formation of soliton-like excitations was observed in 3D case. The developed structures are small hollows filled in with BEC atoms of much greater density compared to surrounding array sites. Figure 13 illustrates the emergence of spatial structures with high atomic concentration in a 3D BEC array, shown as a section along the main diagonal of the cubic domain with $L = 12\pi$. The time interval is selected to display the emergence of soliton-like excitations at $t \sim 28$, and their subsequent decay. The relative atomic

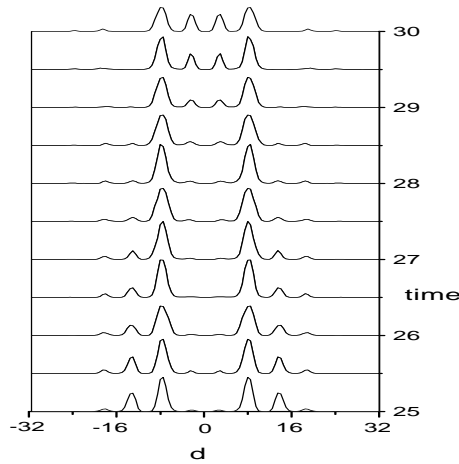


Figure 13. Formation of soliton-like excitations by $t \sim 28$ in a 3D BEC array. d is the distance along the main diagonal of the cubic domain with $L = 12\pi$. The initial condition is $\psi(x, y, z, 0) = 0.5 \sin(x) \sin(y) \sin(z)$.

density in a localized excitation is estimated, as in the 2D case, by numerical integration of $|\psi(x, y, z, t)|^2$ at $t = 28$ over individual lattice sites. In the 3D case $\sim 67\%$ of all the BEC matter, initially uniformly distributed over 1728 lattice sites, are collected in eight sites due to the modulational instability, therefore $n_h = \frac{1728}{8} \cdot 0.67 \cdot n_0 \sim 145n_0$.

For the considered initial parameter settings the long-term evolution of the atomic

distribution over the optical lattice in both 2D and 3D cases exhibits the recurrence phenomenon, which reveals itself as the return to the primary low density state. In order to prevent the decay of soliton-like excitations, similarly to 2D case, the strength of the periodic potential has to be increased adiabatically when the excitations are formed, e.g. at $t \sim 28$ for the above 3D parameter settings (figure 13).

As far as the initial state is concerned, we remark that it could be experimentally realized starting from a uniform condensate with quasi-momentum $k = 0$ (i.e. with equally filled potential wells), and accelerating the optical lattice in a particular direction. The acceleration of the lattice, being equivalent to a gravitational field, will induce the initial $k = 0$ state to move along the band, until it reaches the edge of the band where the instability develops. Depending on the direction selected in the real space (this corresponding to a fixed direction in the reciprocal space), one will get different final localized states from the band edge instability. The issues relevant to preparation of particular Bloch states of the condensate in an optical lattice are discussed in [9].

It should be pointed out that the similarity of the development of modulational instability in all three dimensions is the result of separability of the periodic trap potential. Although this corresponds to the majority of experimental situations, the case of non-separable potentials (non-orthogonal lattices) represents a significant interest.

5. Conclusions

We have studied the modulational instability in arrays of BEC confined to optical lattices. The formation of coherent spatial structures with BEC is shown to be the principal feature of the evolution of atomic distribution over the optical lattice, when guided by the modulational instability. In 1D case the developed structures are the matter-wave solitons which may be regarded as thin disks of highly concentrated BEC atoms. Depending on significance of the nonlinearity, two distinct types of matter-wave solitons may develop, these being the envelope solitons (weak nonlinearity) occupying few lattice sites and intrinsic localized modes (strong nonlinearity), each fitting a single lattice site. In 2D and 3D cases the emerging spatial structures with BEC represent soliton-like excitations regularly arranged over the optical lattice which are, however, not stable. We proposed a simple way to stabilize these localized excitations by increasing the strength of the optical lattice when they are formed due to the modulational instability. Different initial waveforms, corresponding to particular points on the BZ are tested for instability. The aspects of developed spatial structures with BEC is shown to depend on the selected Bloch state. Theoretical model, based on the multiple scale expansion describes the primary features of emerging soliton-like structures with BEC, including the number of localized excitations, their spatial symmetry and relative density of BEC atoms they contain. The proposed method for creation and preserving of soliton-like spatial structures with highly concentrated BEC atoms, may be of interest for the physics and applications of BEC.

Acknowledgments

V.V.K. acknowledges support from the Programme "Human Potential - Research Training Networks", contract No. HPRN-CT-2000-00158. M.S. and B.B. thank the MURST-PRIN-2000 Initiative and the European grant LOCNET n.o HPRN-CT-1999-00163 for partial financial support.

References

- [1] Anderson B P and Kasevich M 1998 *Science* **282** 1686
- [2] Morsch O, Müller J H, Cristiani M, Ciampini D and Arimondo E 2001 *Phys. Rev. Lett.* **87** 140402
- [3] Cataliotti F S, Burger S, Fort C, Maddaloni P, Minardi F, Trombettoni A, Smerzi A and Inguscio M 2001 *Science* **293** 843
- [4] Greiner M, Mandel O, Esslinger T, Hänsch T W and Bloch I 2002 *Nature* **415** 6867
- [5] Greiner M, Bloch I, Mandel O, Hänsch T W and Esslinger T 2001 *Phys. Rev. Lett.* **87** 160405
- [6] Wu B, Diener R B and Niu Q 2002 *Phys. Rev. A* **65** 025601
- [7] Steel M J and Zhang W 1998 *Preprint cond-mat/9810284*
- [8] Konotop V V and Salerno M 2002 *Phys. Rev. A* **65** 021602
- [9] Denschlag J H, Simsarian J E, Häffner H, McKenzie C, Browaeys A, Cho D, Helmerson K, Rolson S L and Phillips W D 2002 *J. Phys. B: At. Mol. Opt. Phys.* **35** 3095
- [10] Tsukada N 2002 *Phys. Rev. A* **65** 063608
- [11] Carusotto I, Embriaco D and La Rocca G C 2002 *Phys. Rev. A* **65** 053611
- [12] Alfimov G L, Konotop V V and Salerno M 2002 *Europhys. Lett.* **58** 7
- [13] Pötting S, Meystre P and Wright E M 2000 *Preprint cond-mat/0009289*
- [14] Dalfovo F, Giorgini S, Pitaevskii L P and Stringari S 1999 *Rev. Mod. Phys.* **71** 463
- [15] Khaykovich L, Schreck F, Ferrari G, Bourdel T, Cubizolles J, Carr L D, Castin Y and Salomon C 2002 *Science* **296** 1290
- [16] Strecker K E, Partridge G B, Truscott A G and Hulet F G 2002 *Nature* **417** 150
- [17] Carr L D and Castin Y 2002 *Preprint cond-mat/0205624*
- [18] Robins N P, Zhang W, Ostrovskaya E A and Kivshar Y S 2001 *Phys. Rev. A* **64** 021601
- [19] Smerzi A, Trombettoni A, Kevrekidis P G and Bishop A R 2002 *Phys. Rev. Lett.* **89** 170402
- [20] Benjamin T B and Feir J E 1967 *J. Fluid Mech.* **27**, 417
- [21] Taniuti T and Washimi H 1968 *Phys. Rev. Lett.* **21** 209
- [22] Askar'yan G A 1962 *Sov. Phys. JETP* **15** 1088
- [23] Ostrovskii L A 1967 *Sov. Phys. JETP* **24**, 797
- [24] Karpman V I 1967 *JETP Lett.* **6** 227
- [25] Kuznetsov E A, Rubenchik A M and Zakharov V E 1986 *Phys. Rep.* **142** 103
- [26] Berge L 1998 *Phys. Rep.* **303** 259
- [27] Akhmediev N N and Ankievich A 1997 *Solitons: Nonlinear Pulses and Beams* (Chapman and Hall, London)
- [28] Belokolos E D, Eilbeck J C, Enolskii V Z and Salerno M 2001 *J. Phys. A: Math. Gen.* **34** 943
- [29] Smerzi A, Fantoni S, Giovanazzi S and Shenoy S R 1997 *Phys. Rev. Lett.* **79** 4950
- [30] Milburn G J, Corney J, Wright E M and Walls D F 1997 *Phys. Rev. A* **55** 4318
- [31] Raghavan S, Smerzi A, Fantoni S, and Shenoy S R 1999 *Phys. Rev. A* **59** 620
- [32] Press W H, Teukolsky S A, Vetterling W T and Flannery B P 1996 *Numerical Recipes. The Art of Scientific Computing.* (Cambridge University Press)
- [33] Trombettoni A and Smerzi A 2001 *Phys. Rev. Lett.* **86** 2353
- [34] Abdullaev F Kh, Baizakov B B, Darmanyan C A, Konotop V V and Salerno M 2001 *Phys. Rev. A* **64** 043606